Earthquake Engineering and Structural Dynamics

A fibre flexure-shear model for seismic analysis of RC framed structures

Journal:	*Earthquake Engineering and Structural Dynamics*
Manuscript ID:	EQE-08-0151
Wiley - Manuscript type:	Research Article
Date Submitted by the Author:	14-Jun-2008
Complete List of Authors:	Ceresa, Paola; EUCENTRE Petrini, Lorenza; Politecnico di Milano Pinho, Rui; University of Pavia Sousa, Romain; University of Aveiro
Keywords:	fibre element, shear deformations, seismic analysis, reinforced concrete frames

Special Issue on *'Nonlinear Modeling, Analysis, and Simulation for Earthquake Engineering', Earthquake Engineering and Structural Dynamics (EQE)*

A fibre flexure-shear model for seismic analysis of RC framed structures

P. Ceresa[1], L. Petrini[2], R. Pinho[3, §], R. Sousa[4]

[1] *European Centre for Training and Research in Earthquake Engineering (EUCENTRE), Pavia, Italy*
[2] *Department of Structural Engineering, Politecnico di Milano, Milan, Italy*
[3] *Department of Structural Mechanics, Universiy of Pavia, Italy*
[4] *Civil Engineering Department, University of Aveiro, Portugal*

SUMMARY

Whilst currently existing modelling approaches of reinforced concrete behaviour allow a reasonably accurate prediction of flexural response, the determination of its shear counterpart needs further developments. There are various modelling strategies in literature able to predict the shear response and the shear-flexure coupling under monotonic loading conditions. However, very few are the reported models that have demonstrated successful results under cyclic loading, as in the seismic load case. These considerations lead to this research work focused on the development of a flexure-shear model for reinforced concrete beam-column elements. A reliable constitutive model for cracked reinforced concrete subjected to cyclic loading was implemented as bi-axial fibre constitutive model into a two-dimensional Timoshenko beam-column element. Aim of this research work is to arrive at the definition of a numerical model sufficiently accurate and, at the same time, computationally efficient, that will enable implementation within a Finite Element package for nonlinear dynamic analysis of existing non seismically designed RC structures that are prone to shear-induced damage and collapse.

KEY WORDS: fibre element, shear deformations, seismic analysis, reinforced concrete frames

1. INTRODUCTION

In past earthquakes, many reinforced concrete (RC) buildings and bridges failed catastrophically due to shear deficiencies of columns and piers. Current design codes have provisions to prevent brittle shear failure, as well as to recognise the influence of flexure ductility demand in shear resistance. However, the accurate simulation of behaviour of existing RC structures subjected to strong ground motion is still a challenging and open problem. In particular, the determination of shear strength and deformation response is still far from reaching a mature state of development.

Most of the state-of-the-art on seismic design and assessment procedures proposed recently for common engineering practice requires either static or dynamic nonlinear analyses using frame elements where the nonlinearity is traditionally introduced with one of two main approaches: lumped-plasticity modelling, or distributed-inelasticity modelling (i.e., the so-called fibre beam-column elements).

Several fibre beam-column elements were developed in the last twenty years with capability of reproducing coupled axial force and flexure effects [1, 2, 3]. The fibre approach fits perfectly within the Euler-Bernoulli beam theory and caters for the accurate

---

§ Correspondence to: R. Pinho, Department of Structural Mechanics, Università degli Studi di Pavia, Via Ferrata 1, 27100 Pavia, Italy. Phone: +39 0382 516934; Fax: +39 0382 529131; Email: rui.pinho@unipv.it

description of response of slender flexure-dominated members [e.g. 4] and full structures [e.g. 5]. However, the latter fails when the coupling between shear, axial and bending action becomes important as, for instance, in RC structures with non-slender elements subjected to seismic loading. Recent studies [6 - 16] have attempted to overcome this limitation by introducing into the fibre approach the Timoshenko beam theory, or even a generalised beam theory coupled with multi-axial constitutive laws for material. Researchers working in each of these areas generally have been successful in producing models that yield results of acceptable accuracy for the 1D or 2D cyclic loading. However, they generally require complex calibration. Models that provide accurate simulations of behaviour under 3D general loading conditions, and, specially, under reversed cyclic loading, are somewhat less common.

The present work thus aims at formulating and implementing, in a finite element code, a fibre beam-column model for predicting nonlinear behaviour in shear of RC framed structures. As first step of the research, the assessment of a large number of the available modelling strategies for the analysis of RC structures under shear action due to cyclic loading was carried out. A detailed description of this assessment can be found in [17, 18]. From this literature review, it resulted that the few existing modelling strategies for fibre beam-column elements with shear effects accounted for, present quite different conceptual backgrounds and solution strategies with varying degrees of implementation complexity and calibration requirements. It was also thus apparent that there is perhaps still room for the development of additional numerical models that are not only accurate, but also that can be introduced in general purpose finite elements codes, and whose input relies solely on engineering properties, thus rendering them more widely applicable to a wider range of structural cases, and users.

In order to reach this objective the work was organised in the following different phases, accurately described in the next sections: (i) choice of a reliable constitutive model for cracked RC subjected to cyclic loading, (ii) verification of the constitutive model using experimental data, (iii) development of a flexure-shear model for cracked RC beam-column elements, (iv) implementation of the formulation into a fibre beam-column element, and (v) verification of the flexure-shear beam model in predicting the cyclic response of RC beam-column members and RC shear walls subjected to axial force, flexure and shear.

2. THE ADOPTED CONSTITUTIVE FORMULATION

Several theories for cracked reinforced concrete subjected to shear are present in the literature [19 - 25]. After a careful review of such literature, the Modified Compression Field Theory (MCFT), and one of its refinements, represented by the Disturbed Stress Field Model (DSFM), stood out as one of those models that seemed capable of accurately predicting the shear strength of both reinforced- and prestressed concrete members subjected to monotonic loads [20, 25]. Indeed, the procedure (adopting membrane elements) has been shown to lead to quite accurate foresights when compared to experimental test results on RC panels and shear walls. The main assumptions of MCFT can be summarised as follows [26]:

- Cracked RC is treated as an orthotropic material where cracks are smeared and allowed to rotate. The principal strain-stress directions (1, 2) are those corresponding to the average compressive and tensile strains (crack directions).

- Equilibrium, compatibility and constitutive relations for concrete and steel are defined in terms of average strains and stresses.
- Reinforcement is smeared throughout the element perfectly bonded to concrete, and the reinforcement shear stress is negligible.
- Verifications at crack locations are introduced in order to evaluate the admissible shear stress along the crack surface.

In order to enlarge the formulation capability, Vecchio [27] introduced the plastic offsets for modelling cyclic loads. Hence, the constitutive relations for concrete and reinforcing bars were expanded to account for cyclic loading and the plastic strains were introduced as offsets. The elastic components of strains were used to define the effective secant stiffnesses, and Mohr's circle technique was used to track strains experienced during previous loading. Palermo and Vecchio [28] improved the constitutive model of concrete accounting for the nonlinear unloading, linear reloading with degradation of strength and stiffness, and for full/partial loading conditions.

The MCFT formulation for modelling cracked RC under shear loading was adopted as the fibre constitutive model in the proposed modelling strategy, and its implementation was checked through a comparison with the experimental results and the predictions published by Vecchio *et al*. for several shear tests performed on RC panels at the University of Toronto.

2.1 Implementation of the formulation

The implementation of the cyclic formulation of the MCFT refers to the models proposed by Vecchio [27], and the improved relationships for concrete proposed by Palermo and Vecchio [28, 29]. The implementation process was not straightforward since the information about the models were limited and the improvements described in [28, 29] were not numerically stable as recognized by the authors.

The difficulties were mainly related to the plastic strains being stored in memory as plastic offsets, the continuous update of the crack direction during loading, and the lack of a crack-closing model for concrete. Further, there are still some additional issues related to local yielding and accumulation of plastic strains in the reinforcement that are not currently properly captured [30].

During the implementation phase, a number of changes were introduced mainly due to the apparent inconsistencies between the original formulation, the results obtained with the code VecTor2 [31], and the numerical responses published by Vecchio and Palermo [27, 29]. These changes concern mainly the implemented constitutive rules for the opening of the cracks, the nonlinear unloading branch for concrete in tension and the crack-check verification accounting for strain hardening, as described in the following sections with reference to [18].

a) Implemented compatibility and equilibrium conditions

Considering the stress-strain conditions in a RC element (Figure 1) previously subjected to an arbitrary load history, the total strain vector in the *x*-*y* reference system is given by the sum of the elastic and plastic contributions, as follows:

$$\{\varepsilon\} = \{\varepsilon^e\} + \{\varepsilon^p\} \quad (1)$$

Equation (1) works for each reinforcement component and for concrete. Given a stress vector $\{\sigma\} = \{\sigma_{xx}, \sigma_{yy}, \tau_{xy}\}^T$ acting at a point in the RC element (Figure 1), the resulting total strains $\{\varepsilon\}$ of Equation (1) are such to satisfy the following equilibrium condition:

$$\{\sigma\} = [D]\{\varepsilon\} - \{\sigma_o\} \tag{2}$$

where $\{\sigma_o\}$ is the pseudo-stress vector due to the plastic offsets for concrete and reinforcements:

$$\{\sigma_o\} = [D_c]\{\varepsilon_c^p\} + \sum_{i=1}^{n} [D_s]_i \{\varepsilon_s^p\}_i \tag{3}$$

The matrix $[D]$ is the composite material stiffness matrix, fully populated and symmetric:

$$[D] = [D_c] + \sum_{i=1}^{n} [D_s]_i \tag{4}$$

where $[D_c]$ is the concrete material stiffness matrix and $[D_s]_i$ are the reinforcement component material stiffness matrices in the (x, y) directions. Since the MCFT models the reinforced concrete as an orthotropic material in the principal directions (1, 2), it is necessary to formulate the material stiffness matrices relative to these directions - $[D_c]'$ and $[D_s]_i'$, respectively.

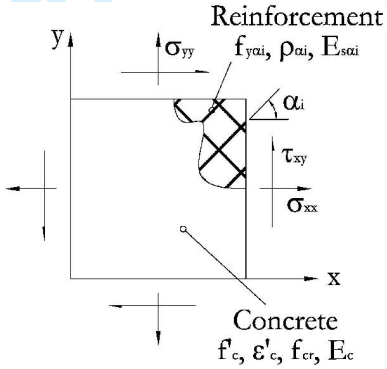

Figure 1. RC membrane element

Standard transformation matrices - $[T_c]$ and $[T_s]_i$ - are then required to rotate from (1, 2) to (x, y) directions for concrete, and from α_i to (x, y) directions for each *i-th* reinforcement component. The rotation angle in $[T]$ matrix is equal to angle θ° of the principal elastic strain directions (1, 2) for concrete, and to α_i for each steel component, leading to the following material matrices:

$$[D_c] = [T_c]^T [D_c]' [T_c] \quad \text{and} \quad [D_s]_i = [T_s]_i^T [D_s]_i' [T_s]_i \tag{5}$$

Assuming that the Poisson's effect is negligible, the material stiffness matrix for concrete evaluated with respect to the principal directions (1, 2) is computed as in Equation (6), on the left. For each steel component, whose ratio is $\rho_{\alpha i}$, the material matrix in the α_i direction is derived as in Equation (6), on the right:

$$[D_c]' = \begin{bmatrix} \overline{E}_{c1} & 0 & 0 \\ 0 & \overline{E}_{c2} & 0 \\ 0 & 0 & \overline{G}_c \end{bmatrix} \qquad [D_s]_i' = \begin{bmatrix} \rho_{\alpha i}\overline{E}_{s\alpha i} & 0 & 0 \\ 0 & 0 & 0 \\ 0 & 0 & 0 \end{bmatrix} \tag{6}$$

The secant moduli are related to a particular state of stress and elastic strain as follows:

$$\overline{E}_{c1}= f_{c1} / \varepsilon^{e}_{c1}, \quad \overline{E}_{c2}= f_{c2} / \varepsilon^{e}_{c2}, \quad \overline{G}_{c} = \frac{\overline{E}_{c1} \cdot \overline{E}_{c2}}{\overline{E}_{c1} + \overline{E}_{c2}}, \quad \overline{E}_{s\alpha i} = f_{s\alpha i} / \varepsilon^{e}{}_{s\alpha i} \tag{7}$$

Working in the directions *x*-*y*, the plastic offsets of the each reinforcement component are computed as a function of the plastic strain $\varepsilon^{p}_{s\alpha i}$ in the direction α_i:

$$\left\{\varepsilon^{p}_{s}\right\}_{i} = \begin{Bmatrix} \varepsilon^{p}_{sxi} \\ \varepsilon^{p}_{syi} \\ \gamma^{p}_{sxyi} \end{Bmatrix} = \begin{Bmatrix} \varepsilon^{p}_{s\alpha i} \cdot \left(1+\cos 2\alpha_i\right)/2 \\ \varepsilon^{p}_{s\alpha i} \cdot \left(1-\cos 2\alpha_i\right)/2 \\ \varepsilon^{p}_{s\alpha i} \cdot \left(\sin 2\alpha_i\right) \end{Bmatrix} \tag{8}$$

The concrete plastic strain vector is calculated in the directions *x*-*y* using standard transformation of Mohr's circle of strains, as it will be explained later:

$$\left\{\varepsilon^{p}_{c}\right\} = \begin{Bmatrix} \varepsilon^{p}_{cx} \\ \varepsilon^{p}_{cy} \\ \gamma^{p}_{cxy} \end{Bmatrix} = \begin{Bmatrix} \varepsilon^{p}_{cxold} + \dfrac{\Delta\varepsilon^{p}_{c1}}{2}(1+\cos 2\theta^{e}) + \dfrac{\Delta\varepsilon^{p}_{c2}}{2}(1-\cos 2\theta^{e}) \\ \varepsilon^{p}_{cyold} + \dfrac{\Delta\varepsilon^{p}_{c1}}{2}(1-\cos 2\theta^{e}) + \dfrac{\Delta\varepsilon^{p}_{c2}}{2}(1+\cos 2\theta^{e}) \\ \gamma^{p}_{cxyold} + \Delta\varepsilon^{p}_{c1}(\sin 2\theta^{e}) - \Delta\varepsilon^{p}_{c2}(\sin 2\theta^{e}) \end{Bmatrix} \tag{9}$$

where ε^{p}_{cxold}, ε^{p}_{cyold}, γ^{p}_{cxyold} are the previous plastic strains, $\Delta\varepsilon^{p}_{c1}$ and $\Delta\varepsilon^{p}_{c2}$ are the increments of the plastic strains in directions (1, 2) occurring at a given load step. It has to be pointed out that the compressive or tensile response may occur in either of the principal strain directions (i.e., $\varepsilon_c = \varepsilon_{c1}$ or $\varepsilon_c = \varepsilon_{c2}$); the other parameters, in terms of strains and stresses, are subscripted accordingly.

b) Implemented material relationships

Figure 2 shows the adopted cyclic reinforcement model, proposed by Vecchio [27]. The monotonic envelope is tri-linear with a linear strain hardening portion after the yield plateau. The hysteretic response has been modelled after Seckin [32], and the Bauschinger effect is represented by a Ramberg-Osgood formulation.

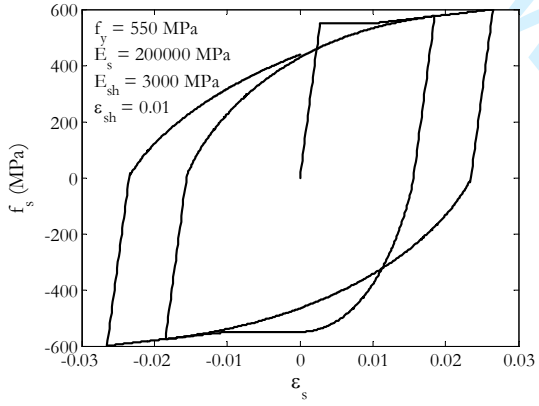

Figure 2. Hysteretic model for reinforcement, according to [27]

The cyclic stress-strain relation for concrete can be described using three types of curves: the compressive envelope curve, the tensile envelope curve, and the unloading/reloading

curve that connects the two envelope curves. The compressive envelope curve follows the Popovics formulation and accounts for compression softening [33]. Concerning concrete in tension, the behaviour is linear elastic before cracks appear; a nonlinear descending branch then follows when cracks form taking into account the tension stiffening effect. The shape and slope of the unloading and reloading responses are dependent on the plastic offset strains. The plastic offset is used as parameter in defining the unloading path and in determining the degree of damage in the concrete due to cycling.

Two different models have been followed for defining the trend of the unloading/reloading paths as shown in Figure 3 [18], where ε_c' is the peak compressive strain and f_c' is the corresponding stress, and f_t' is the tensile strength of concrete: on the left, the response obtained following the Vecchio model [27]; on the right, the one related to Palermo and Vecchio model [29]. In the numerical applications described in Section 4, however, only the linear unloading/reloading paths were employed, given that numerical problems were encountered when using their nonlinear counterparts [29].

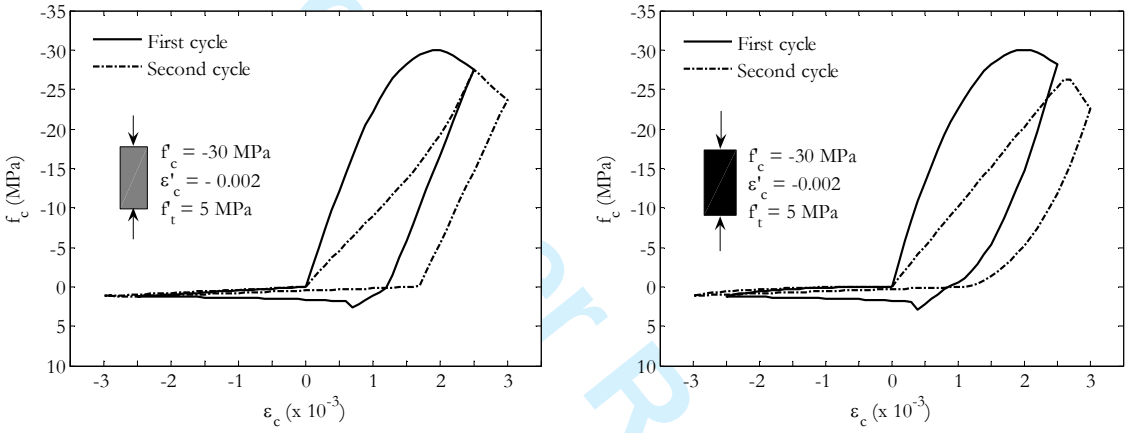

Figure 3. Response of an element subjected to uniaxial strain excursions with the implemented models for concrete

The implemented cyclic compressive rules based on the Vecchio model [27] are depicted in Figure 4, where ε_{cm} is the maximum compressive strain attained during previous loading and f_{cm} the corresponding stress, ε_p is the strain corresponding to the peak stress in the base curve, and β is a reduction factor that reflects the softening effect of principal tensile strains.

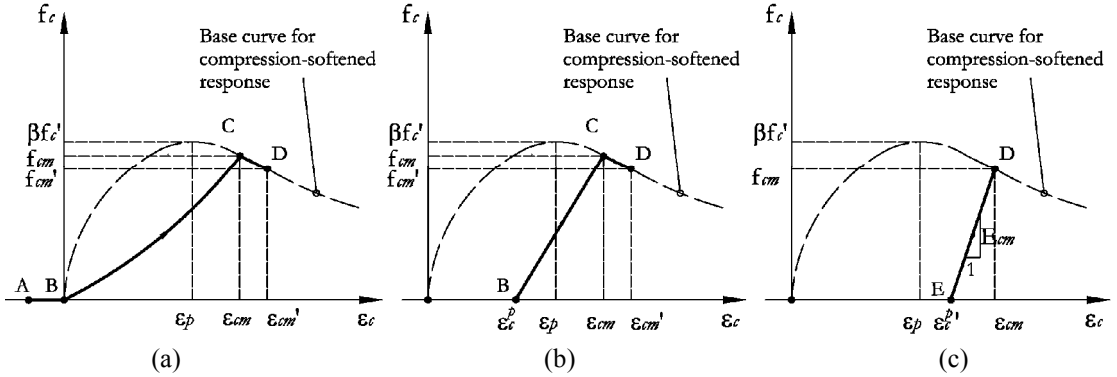

Figure 4. Implemented (a), (b) reloading and (c) unloading paths for concrete in compression (adapted from [27])

At each load stage, the instantaneous plastic strain corresponding to a total strain ε_c is calculated with Equation (10), derived by Vecchio [27] through regression analyses of extensive experimental data:

$$\varepsilon_c^p = \begin{cases} \varepsilon_c - \varepsilon_p\left[0.87\left(\varepsilon_c/\varepsilon_p\right) - 0.29\left(\varepsilon_c/\varepsilon_p\right)^2\right] & if\ \varepsilon_c > 1.5\varepsilon_p \\ \varepsilon_c - 0.001305\left(\varepsilon_p/0.002\right) & if\ \varepsilon_c < 1.5\varepsilon_p \end{cases} \quad (10)$$

According to the theory proposed by Vecchio [27], the cyclic tensile rules of concrete are linear, as shown in Figure 5 where ε_{tm} is the maximum previously attained tensile strain, f_{tm} is the corresponding stress and ε_c^p is the current plastic offset strain computed as in Equation (11) or is equal to the compressive plastic strain in Equation (10) if tensile stresses develop under compressive straining. In Vecchio's formulation, no positive offsets were considered due to the lack of a suitable model, as shown in Figure 5:

$$\varepsilon_c^p = 0 \quad (11)$$

Shown in Figure 3 and Figure 5 are the implemented constitutive rules for the opening of cracks. If concrete is damaged during the compression at the initial loading, tensile cracking would occur at the compressive strain due to the residual plastic strain developed by the initial compressive loading. After the first unloading, the tensile base curve is shifted such that it coincides with the plastic offset calculated from the compressive regime.

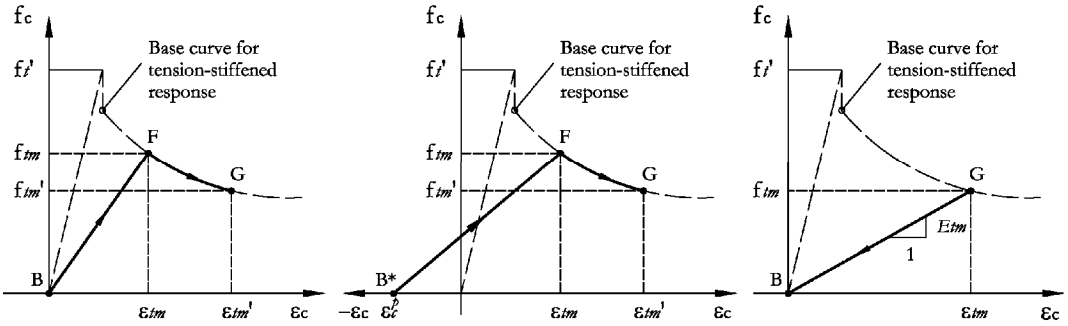

(a) (b) (c)

Figure 5. Implemented (a), (b) reloading and (c) unloading paths for concrete in tension (adapted from [27])

In particular, the tensile strength and strain are computed as a function of the previous maximum compressive strain, ε_{cm}, and of the strain at which the unloading curve reaches the strain axis, ε_c^p, according to the formulation proposed by Steven *et al.* [34]:

$$f_t'^* = f_t'/a, \quad \varepsilon_t'^* = \varepsilon_c^p + f_t'^*/E_{cr}^*, \quad \text{with } a = (1 + 0.30\,(\varepsilon_{cm}/\varepsilon_p)^4) \quad (12)$$

where f_t' is the maximum tensile strength for undamaged concrete, ε_p is the strain corresponding to the peak compressive stress in the base curve, ε_c^p is the compressive plastic deformation of Equation (10). Knowing the Young modulus E_c of undamaged concrete, the parameter E_{cr}^* is the stiffness of the linear tensile curve up to $f_t'^*$:

$$E_{cr}^* = E_c\,(0.98 - 0.70\cdot(\varepsilon_{cm}/\varepsilon_p)^{0.41}) > 0.05\,E_c \quad (13)$$

c) Implemented deformation updating rules

When considering constitutive relationships for concrete, the pertinent strain directions are those parallel to the principal elastic concrete strains, whose inclination is θ^e (Figure 6a). However, these axes rotate as the load changes. As such, a critical requirement of the cyclic formulation is to define and retain in memory the concrete plastic and maximum strains and their strain envelopes with respect to the *x*-*y* axes, and transform them to and from arbitrary orientations of the principal directions using Mohr's circle approach (Figure 6b). The latter is used to track strains experienced during previous loading, considering the continuous changing of the principal directions.

As introduced in Equation (9), the update of the plastic strains is computed as a function of the increments (which may be positive or negative) $\Delta\varepsilon_{c1}^{p}$ and $\Delta\varepsilon_{c2}^{p}$, and the orientation θ^e. Similarly, the maximum compressive strains ε_{cmx}, ε_{cmy}, γ_{cmxy} and the maximum tensile strains ε_{tmx}, ε_{tmy}, γ_{tmxy} are updated, knowing the compressive and tensile increments $-\Delta\varepsilon_{cm1}$, $\Delta\varepsilon_{cm2}$ and $\Delta\varepsilon_{tm1}$ $\Delta\varepsilon_{tm2}$, respectively – and the orientation θ^e. Mohr's circle relationships transform them from the reference axes *x*-*y* to the principal elastic strains directions 1-2 whose orientation is θ^e, and vice-versa.

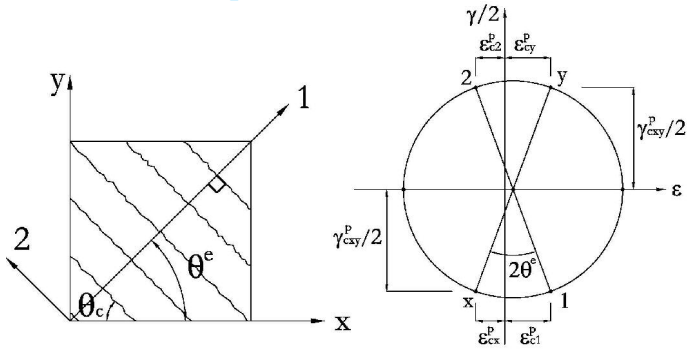

(a) (b)

Figure 6. Defining envelopes of concrete strains using Mohr's circle: (a) principal axes in cracked concrete, and (b) plastic strain

2.2 Verification of the implemented formulation

The implemented formulation was checked firstly through a comparison with the experimental results and the numerical predictions published by Vecchio *et al*. [20, 27, 29, 34-36, 37] for several shear tests performed on RC panels tested at the University of Toronto, under monotonic and cyclic load histories. Moreover, the comparison was also made with the results of the code VecTor2: it is a finite element program developed by Vecchio [31], where the monotonic and cyclic formulations of the MCFT are implemented. These comparisons gave the possibility to identify some inconsistencies between the theory originally proposed by Vecchio *et al.*, the numerical predictions published by the latter and the results obtained with the more recent and certainly more up-to-date code VecTor2.

In particular, the reproduction of the test results of several RC panels and membrane elements subjected to monotonic loading has been carried out without any modification of the formulations originally proposed for the MCFT/DSFM. The material constitutive models were implemented taking into account all the aspects described in the MCFT/DSFM formulations (i.e., compression softening, tension stiffening, local checks

at crack location, etc). As reported in Ceresa [18], good agreement was found with both the observed response and the numerical predictions published by Vecchio *et al.*

The verification of the implemented cyclic formulation was carried out reproducing the response of RC panels tested at the University of Toronto by Stevens *et al*. [34] and Villani [37]. Good agreement was verified between the implemented formulation and the response obtained with the code VecTor2, while discrepancies were found with the numerical predictions published in literature [27, 29].

In the majority of analysed cases, the MCFT theory proved to be capable of reproducing the fundamental aspects of the experimental responses for both monotonic and cyclic loading conditions (as shown in Section 4). However, some additional issues related to the local accumulation of strains in the reinforcement, the tensile plastic strain and, hence, the crack closing model for concrete, are not currently captured in a proper way, and will require further investigations.

3.IMPLEMENTATION OF THE FLEXURE-SHEAR MODEL

After the choice of the constitutive models, the next steps were the development of the sectional formulation, and the implementation of the proposed flexure-shear model into a fibre beam-column finite element. A two-dimensional Timoshenko fibre beam-column element was developed.

3.1 Section state determination

Considering the cross section depicted in Figure 7, the stresses and strains of each i-*th* fibre are related by means of the following constitutive relations:

$$\begin{Bmatrix} \sigma_{xx} \\ \sigma_{yy} \\ \tau_{xy} \end{Bmatrix}^i = \begin{bmatrix} D_{11} & D_{12} & D_{13} \\ D_{21} & D_{22} & D_{23} \\ D_{31} & D_{32} & D_{33} \end{bmatrix}^i \begin{Bmatrix} \varepsilon_{xx} \\ \varepsilon_{yy} \\ \gamma_{xy} \end{Bmatrix}^i - \begin{Bmatrix} \sigma_{oxx} \\ \sigma_{oyy} \\ \tau_{oxy} \end{Bmatrix}^i \tag{14}$$

which can be rewritten in compact form as:

$$\boldsymbol{\sigma}^i = \mathbf{D}^i \boldsymbol{\varepsilon}^i - \boldsymbol{\sigma}_o^i \tag{15}$$

where $\boldsymbol{D}^i$ is the composite material stiffness matrix in the reference system *x*-*y*, and $\boldsymbol{\sigma}_o^i$ is the pseudo-stress vector accounting for prestrains (i.e. plastic deformations, elastic offsets, strains due to shear slip).

For the determination of the fibre strains, the following hypotheses were introduced. With the plane section assumption, the axial strain (ε_{xx}) is known for each fibre. Assuming that the shear strain is uniform along the section according to the Timoshenko beam theory, the shear distortion (γ_{xy}) components of the strain field are calculated for the entire section (for all the fibres, as shown in Figure 7, on the right). Accordingly, each fibre has two input variables, axial strain (ε_{xx}) and shear distortion (γ_{xy}), based on the element deformations – axial deformation (ε_o), section curvature (χ) and shear deformation (γ_o). The only unknown is the transversal strain within each fibre (ε_{yy}). The latter is initially guess-estimated to complete the definition of the strain field, allowing stresses and forces to be determined from the constitutive material relationships and geometric properties for each fibre (dimensions, concrete properties and reinforcement

percentages). For the initial estimate of the transversal strain ε_{yy} within each fibre, the resulting strain value from the previous load step was used.

It has been assumed that transversal stress within each fibre is equal to zero. Therefore, the transverse strain ε^i_{yy} is iteratively determined for each fibre as follows:

$$\sigma^i_{yy} = 0 \quad \Rightarrow \quad \varepsilon^i_{yy} = \left(-\frac{\varepsilon_{xx} D_{21} + \gamma_{xy} D_{23}}{D_{22}} + \frac{\sigma_{oyy}}{D_{22}} \right)^i \tag{16}$$

where D_{21}, D_{22}, D_{23} are the coefficients of the composite material matrix [D], and σ_{oyy} is the transversal component of the pseudo-stress vector $\boldsymbol{\sigma}_o^i$ of Equation (3). It results that the transversal strain is expressed as a function of both axial and shear deformations and, additionally, of the transversal component σ_{oyy} of the pseudo-stress vector where the plastic deformations are accounted for.

Once the equilibrium in the transverse direction is achieved within a specific tolerance error for each fibre, the static condensation of Equation (14) leads to the determination of the axial and shear stresses for each fibre:

$$\begin{Bmatrix} \sigma_{xx} \\ \tau_{xy} \end{Bmatrix}^i = \begin{bmatrix} k_{11} & k_{12} \\ k_{21} & k_{22} \end{bmatrix}^i \begin{Bmatrix} \varepsilon_{xx} \\ \gamma_{xy} \end{Bmatrix}^i + \begin{Bmatrix} -\sigma_{oxx} + \sigma_{oyy}\alpha_{12} \\ -\tau_{oxy} + \sigma_{oyy}\alpha_{32} \end{Bmatrix}^i \tag{17}$$

where k_{11}, k_{12}, k_{21}, k_{22} are the coefficients of the condensed composite material matrix (2×2), and $\alpha_{12} = D_{12}/D_{22}$, and $\alpha_{32} = D_{32}/D_{22}$. The condensed composite stiffness matrix establishes a direct coupling between the axial and the shear strains, and therefore between axial and shear stresses at sectional level.

The iterative procedure for the section state determination is fully described in the flowchart in Figure 7. It must be pointed out that in this kind of model the bulk of the computational demand is the fibre state determination (i.e., constitutive behavior monitoring).

3.2 Implementation of a displacement-based Timoshenko fibre beam element

The element state determination is schematically described in Figure 7. The developed fibre beam-column element has been implemented in FEAPpv [38].

The sectional model previously described has been adopted for the development of a two-dimensional fibre beam element. A classical displacement-based approach was followed: the displacement fields are approximated with the product of the shape functions by the corresponding nodal displacements. In the case of a 2D finite element, three are the degrees of freedom (DOFs) per node – the axial $u(x)$ and transversal $v(x)$ displacements, and the rotation $\theta_z(x)$, all of which approximated through linear shape functions:

$$\begin{cases} u(x) = \mathbf{N}^{\mathbf{u}}(x) \cdot \hat{\mathbf{u}} \\ v(x) = \mathbf{N}^{\mathbf{v}}(x) \cdot \hat{\mathbf{v}} \\ \theta_z(x) = \mathbf{N}^{\boldsymbol{\theta}_z}(x) \cdot \hat{\boldsymbol{\theta}}_{\mathbf{z}} \end{cases} \tag{18}$$

where $\hat{\mathbf{u}}$, $\hat{\mathbf{v}}$ and $\hat{\boldsymbol{\theta}}_{\mathbf{z}}$ are the nodal DOFs corresponding respectively to the longitudinal, transverse displacements and to the rotation, and x is the beam axis whose cross-section is in the y-z plane and length is l, and the shape-functions are set as:

$$\mathbf{N}^{\mathbf{u}}(x) = \mathbf{N}^{\mathbf{v}}(x) = \mathbf{N}^{\boldsymbol{\theta}_z}(x) = \left\{1 - \frac{x}{l},\ \frac{x}{l}\right\} \tag{19}$$

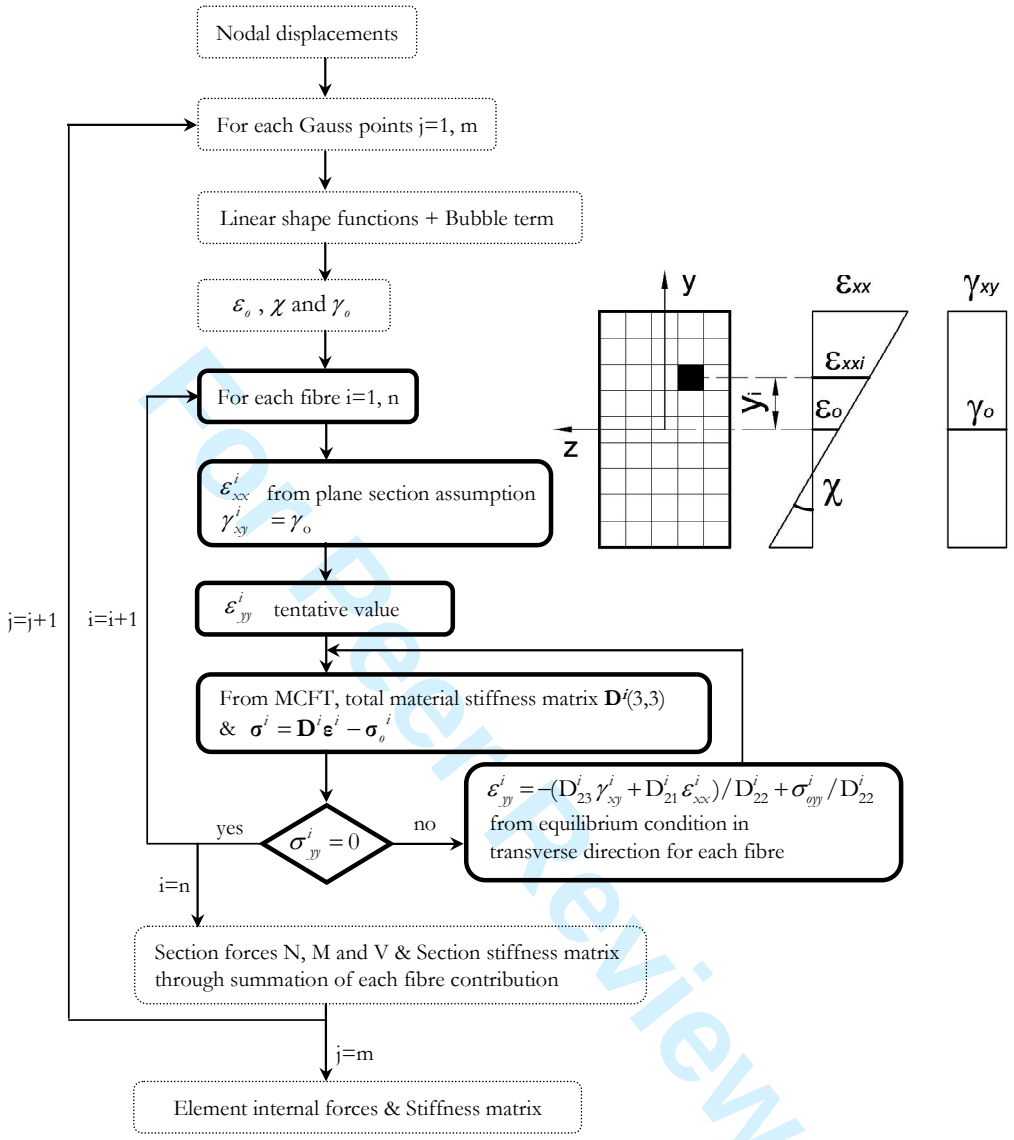

Figure 7. Element state determination of the displacement-based Timoshenko fibre element

According to the Timoshenko assumption that cross-sections remain plane but not necessarily normal to the deformed longitudinal axis, the shear deformation is derived from:

$$v'(x) - \theta_z(x) \neq 0 \quad \rightarrow \varepsilon_{xy}(x) \neq 0 \tag{20}$$

Using the shape functions of Equation (19) and their first derivatives, the shear strain $\gamma_{xy}(x) = 2\ \varepsilon_{xy}(x)$ can be computed as follows:

$$\gamma_{xy}(x) = \mathbf{B}^{\mathbf{v}}(x)\ \hat{\mathbf{v}} - \mathbf{N}^{\boldsymbol{\theta}_z}(x)\hat{\boldsymbol{\theta}}_z \tag{21}$$

The Timoshenko beam finite element with linear interpolation of both transverse deflection $v(x)$ and rotation $\theta_z(x)$ is the simplest possible element formulation. However,

it leads to very stiff response predictions for slender beams, i.e. as the length-to-thickness ratio becomes large. Such behaviour is known as shear locking [39], and it is due to the inability of the element to represent a constant state of transverse shear strain γ_{xy}. The locking is due to the inconsistency of the interpolation used for $v(x)$ and $\theta_z(x)$.

In order to overcome the shear-locking problem, the element formulation described earlier was improved using the linear shape functions of Equation (19) for all displacement fields with the addition of a linked term, or *bubble function* N_b, for the transversal displacement field, following the formulation proposed by Auricchio [40]:

$$\begin{cases} u(x) = \mathbf{N}^{\mathbf{u}}(x)\,\hat{\mathbf{u}}, \\ v(x) = \mathbf{N}^{\mathbf{v}}(x)\,\hat{\mathbf{v}} + N_b(\hat{\theta}_{z1} - \hat{\theta}_{z2})l = \mathbf{N}^{\mathbf{v}}(x)\,\hat{\mathbf{v}} + N_b\, l(\mathbf{b}\cdot\hat{\boldsymbol{\theta}}_{\mathbf{z}}), \\ \theta_z(x) = \mathbf{N}^{\boldsymbol{\theta}\mathbf{z}}(x)\,\hat{\boldsymbol{\theta}}_{\mathbf{z}} \end{cases} \tag{22}$$

Hence, the shear deformation can be derived as follows:

$$\gamma_{xy}(x) = \mathbf{B}^{\mathbf{v}}(x)\hat{\mathbf{v}} - \mathbf{N}^{\boldsymbol{\theta}\mathbf{z}}(x)\hat{\boldsymbol{\theta}}_{\mathbf{z}} + \mathbf{D}_{\mathbf{b}}(x)\hat{\boldsymbol{\theta}}_{\mathbf{z}} \tag{23}$$

with the introduction of the following quantities:

$$\begin{gathered} \mathbf{b} = (1, -1), \quad \hat{\boldsymbol{\theta}}_{\mathbf{z}} = (\hat{\theta}_{z1}, \hat{\theta}_{z2})^T, \quad (\mathbf{b}\cdot\hat{\boldsymbol{\theta}}_{\mathbf{z}}) = (\hat{\theta}_{z1} - \hat{\theta}_{z2}), \\ N_b = \frac{1}{2}\left(1 - \frac{x}{l}\right)\cdot\frac{x}{l}, \quad \mathbf{D}^{\mathbf{b}}(x) = \frac{1}{2}\left(1 - \frac{2x}{l}\right)\mathbf{b} \end{gathered} \tag{24}$$

The element stiffness matrix is computed by means of linearisation of the residual functions with respect to the nodal displacements, hence the following terms (2 × 2 sub-matrices) are derived:

$$\mathbf{K}_{\mathbf{uu}} = \int_l \int_A (\mathbf{B}^{\mathbf{u}})^T \frac{\partial \sigma_{xx}}{\partial_{\varepsilon xx}} \mathbf{B}^{\mathbf{u}} dA\, dl;$$

$$\mathbf{K}_{\mathbf{uv}} = \int_l \int_A (\mathbf{B}^{\mathbf{u}})^T \frac{\partial \sigma_{xx}}{\partial \gamma_{xy}} \mathbf{B}^{\mathbf{v}} dA\, dl$$

$$\mathbf{K}_{\mathbf{u\theta}} = \int_l \int_A (\mathbf{B}^{\mathbf{u}})^T \frac{\partial \sigma_{xx}}{\partial \varepsilon_{xx}} y(-\mathbf{B}^{\boldsymbol{\theta}\mathbf{z}}) dA\, dl + \int_l \int_A (\mathbf{B}^{\mathbf{u}})^T \frac{\partial \sigma_{xx}}{\partial \gamma_{xy}} \left[-\mathbf{N}^{\boldsymbol{\theta}\mathbf{z}} + \mathbf{D}^{\mathbf{b}}\right] dA\, dl$$

$$\mathbf{K}_{\mathbf{vu}} = \int_l \int_A (\mathbf{B}^{\mathbf{v}})^T \frac{\partial \tau_{xy}}{\partial \varepsilon_{xx}} \mathbf{B}^{\mathbf{u}} dA\, dl;$$

$$\mathbf{K}_{\mathbf{vv}} = \int_l \int_A (\mathbf{B}^{\mathbf{v}})^T \frac{\partial \tau_{xy}}{\partial \gamma_{xy}} \mathbf{B}^{\mathbf{v}} dA\, dl$$

$$\mathbf{K}_{\mathbf{v\theta}} = \int_l \int_A (\mathbf{B}^{\mathbf{v}})^T \frac{\partial \tau_{xy}}{\partial \varepsilon_{xx}} (-y\mathbf{B}^{\boldsymbol{\theta}\mathbf{z}}) dA\, dl + \int_l \int_A (\mathbf{B}^{\mathbf{v}})^T \frac{\partial \tau_{xy}}{\partial \gamma_{xy}} \left[-\mathbf{N}^{\boldsymbol{\theta}\mathbf{z}} + \mathbf{D}^{\mathbf{b}}\right] dA\, dl$$

$$\mathbf{K}_{\boldsymbol{\theta}\mathbf{u}} = \int_l \int_A (\mathbf{B}^{\boldsymbol{\theta}\mathbf{z}})^T \frac{\partial \sigma_{xx}}{\partial \varepsilon_{xx}} (-y\mathbf{B}^{\mathbf{u}}) dA\, dl + \int_l \int_A \left[\mathbf{D}^{\mathbf{b}} - \mathbf{N}^{\boldsymbol{\theta}\mathbf{z}}\right]^T \frac{\partial \tau_{xy}}{\partial \varepsilon_{xx}} (\mathbf{B}^{\mathbf{u}}) dA\, dl$$

$$\mathbf{K}_{\theta \mathrm{v}} = \int_l \int_A (\mathbf{B}^{\theta z})^T \frac{\partial \sigma_{xx}}{\partial \gamma_{xy}} (-y\mathbf{B}^{\mathrm{v}}) dA\, dl + \int_l \int_A \left[\mathbf{D}^{\mathbf{b}} - \mathbf{N}^{\theta z}\right]^T \frac{\partial \tau_{xy}}{\partial \gamma_{xy}} (\mathbf{B}^{\mathrm{v}}) dA\, dl$$

$$\mathbf{K}_{\theta\theta} = \int_l \int_A (\mathbf{B}^{\theta z})^T \left\{ \frac{\partial \sigma_{xx}}{\partial \varepsilon_{xx}} \left(y^2\, \mathbf{B}^{\theta z}\right) + \frac{\partial \sigma_{xx}}{\partial \gamma_{xy}} (-y) \left[\mathbf{D}^{\mathbf{b}} - \mathbf{N}^{\theta z}\right] \right\} dA\, dl +$$

$$\int_l \int_A \left[\mathbf{D}^{\mathbf{b}} - \mathbf{N}^{\theta z}\right]^T \left\{ \frac{\partial \tau_{xy}}{\partial \varepsilon_{xx}} \left(-y\mathbf{B}^{\theta z}\right) + \frac{\partial \tau_{xy}}{\partial \gamma_{xy}} \left[\mathbf{D}^{\mathbf{b}} - \mathbf{N}^{\theta z}\right] \right\} dA\, dl$$

where the coefficients $\partial\sigma_{xx}/\partial\varepsilon_{xx}$, $\partial\sigma_{xx}/\partial\gamma_{xy}$, $\partial\tau_{xy}/\partial\gamma_{xy}$, and $\partial\tau_{xy}/\partial\varepsilon_{xx}$ are derived from the static condensation in Equation (17). These terms are different from zero due to the adopted flexure-shear fibre model. Therefore, the stiffness matrix directly includes the coupling between flexure and shear contributions. Moreover, the presence of the bubble function introduces additional terms in the stiffness matrix coefficients.
The internal forces are computed as follows:

$$\begin{aligned} F_i^{axial} &= \int_l (\mathbf{B}^{\mathbf{u}})^T N\, dl \\ F_i^{shear} &= \int_l (\mathbf{B}^{\mathrm{v}})^T V\, dl \\ F_i^{bending} &= \int_l [(\mathbf{B}^{\boldsymbol{\theta}})^T M - (\mathbf{N}^{\boldsymbol{\theta}})^T V + (\mathbf{D}^{\mathbf{b}})^T V\,] dl \end{aligned} \tag{25}$$

4.NUMERICAL VERIFICATION OF THE FLEXURE-SHEAR MODEL

The proposed modelling strategy was verified by means of numerical studies and comparisons with experimental results. In particular, the experimental responses of RC columns and shear walls subjected to cyclic loading were taken into account. The response "predictions" obtained with the developed fibre-shear formulation are also compared with the numerical results obtained with a fibre-flexural formulation [41]. In what follows, only a sample of representative results is given, whilst a complete set of case-studies is described in Ceresa *et al.* [42]. Each test specimen will be labelled according to its typology and aspect ratio, as described below.

4.1 Verification against experimental results on short piers with solid cross-section

The flexure-shear formulation was firstly validated by modelling large-scale RC squat columns with full cross-section (labelled as "Col_Solid_"). The numerical predictions of four case-studies are presented in the following. The first application refers to the RC column (Column OA5) tested in Japan by Arakawa *et al*. [43]; a further simulation makes use of the results of the pier whose test was conducted in Japan by Imai and Yamamoto [44]; the third case (Column SC3) is related to the tests performed at the University of Texas by Aboutaha *et al.* [45]; and the final example presented here is a pier (Specimen 3CLH18) belonging to the testing campaign conducted at the University of Berkeley by Lynn [46]; the latter was modelled by Saritas [15] using a different type of fibre model with shear modelling. In the following, the specimens will be named after their aspect ratio as: Col_Solid_1.25, Col_Solid_1.65, Col_Solid_2.67, Col_Solid_3.22, respectively. The applied axial loads, the geometric and mechanical properties of the four case studies

are given in Table I; the lateral loading system displaced three of the columns (Col_Solid_1.25, 1.65 and 3.22) in double bending and the last in single bending.

The force-displacement responses are plotted from Figure 8 to Figure 11, comparing the experimental results with the numerical simulations for the piers, with a fibre-flexure model (on the left) and with the developed fibre-shear model (on the right).

Table I. Geometry and material parameters for non-hollow cross-section squat columns

	Col_Solid_1.25 L = 225 mm	Col_Solid_1.65 L = 825 mm	Col_Solid_2.67 L = 1219.2 mm	Col_Solid_3.22 L = 1473.2 mm
Reference	Arakawa *et al.*[43]	Imai and Yamamoto[44]	Aboutaha *et al.*[45]	Lynn[46]
Scale factor	1:2	1:2	1:1	1:2
Outer perimeter b × h (mm)	180 × 180	400 × 500	914.4 × 457.2	457.2 × 457.2
Aspect ratio L/h	1.25	1.65	2.67	3.22
Axial load (kN)	-476	-392	-	-503
Concrete strength (MPa)	-33.0	-27.1	-21.9	-26.9
Strain at peak stress	-0.0024	-0.0022	-0.002	-0.0022
Concrete elastic modulus (MPa)	26999	24467	21995	24377
Cracking stress (MPa)	1.89	1.72	1.54	1.71
N° Long. bars and ϕ (mm)	8 ϕ 12.7	14 ϕ 22	4 ϕ 25.5 + 12 ϕ 25	8 ϕ 31.75
Long. yielding stress (MPa)	340	318	434	331
Stirrups ϕ and @ (mm)	ϕ 4@ 64.3	ϕ 9@ 100	ϕ 9.53@ 406.4	ϕ 9.5@ 457.2
Trans. yielding stress (MPa)	249	336	400	400

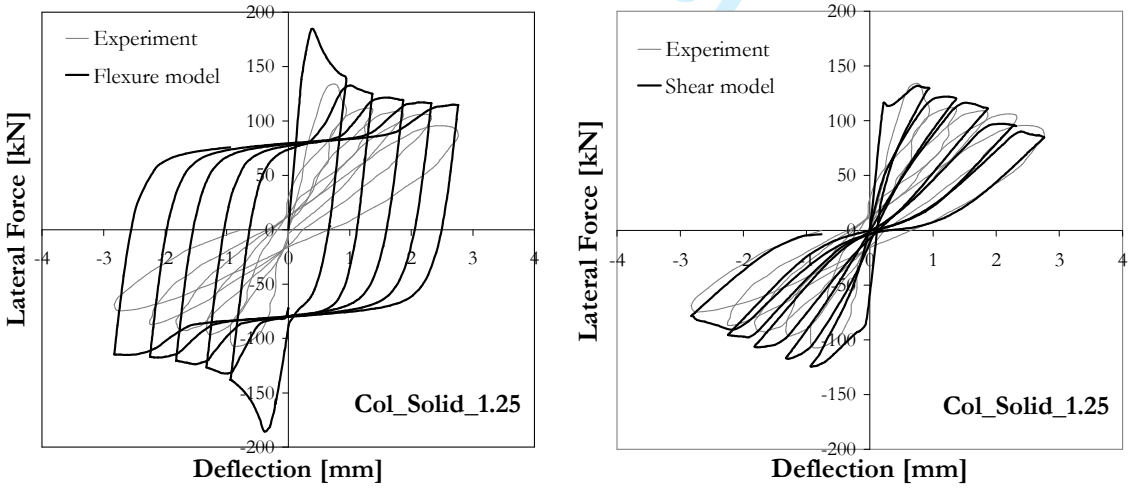

Figure 8. Force-displacement response of specimen Col_Solid_1.25 [43] using a fibre-flexure model (on the left), and the implemented fibre-shear model (on the right)

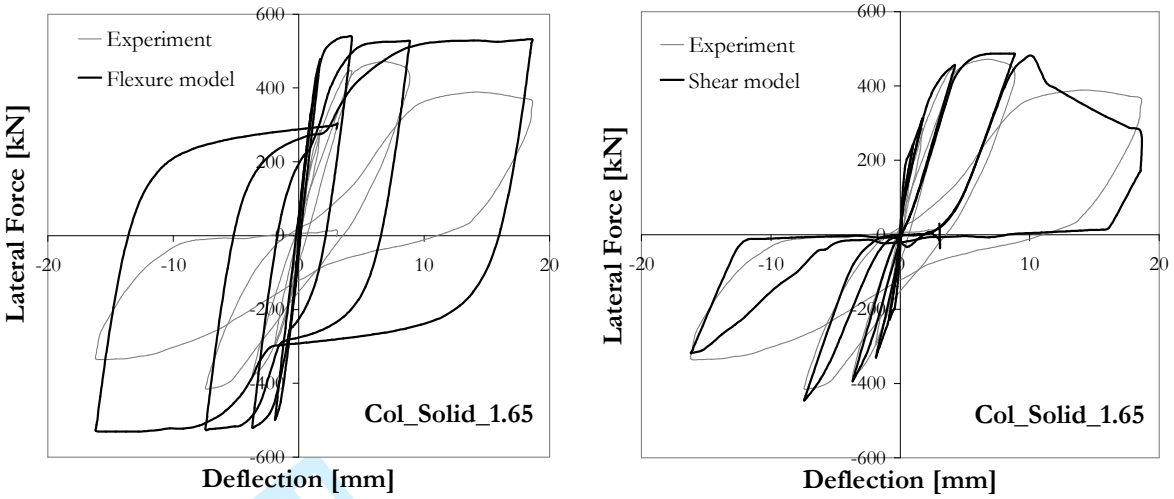

Figure 9. Force-displacement response of specimen Col_Solid_1.65 [44] using a fibre-flexure model (on the left), and the implemented fibre-shear model (on the right)

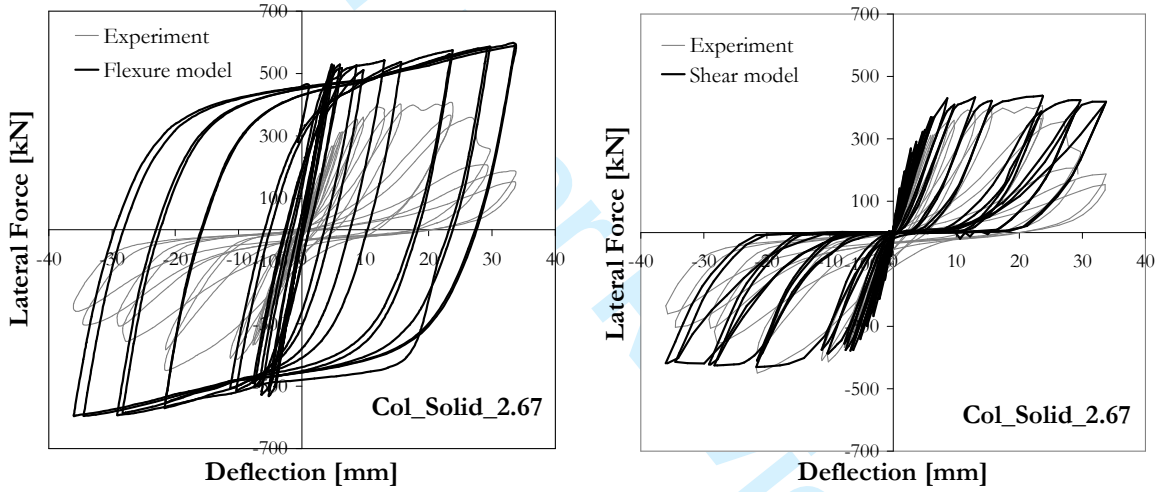

Figure 10. Force-displacement response of specimen Col_Solid_2.67 [45] using a fibre-flexure model (on the left), and the implemented fibre-shear model (on the right)

Comparisons with the experimental results show significant improvement in response predictions when the flexural formulation is replaced by the developed fibre-shear formulation. Even if the latter leads to an overestimation of the initial stiffness and an exaggerating pinching effect, the predicted response shows a better agreement with the measured behaviour in terms of both energy dissipation and shear capacity. The experimentally observed lateral strength degradation is well captured for specimens Col_Solid_1.25 and Col_Solid_1.65, whereas the ultimate lateral load is not well reproduced for the Col_Solid_2.67 and Col_Solid_3.22 case-studies.

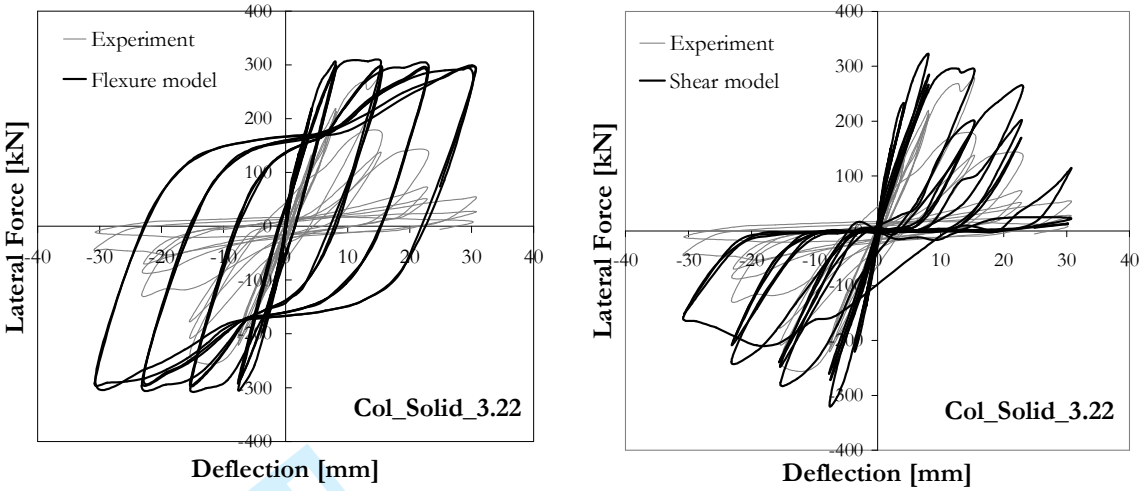

Figure 11. Force-displacement response of specimen Col_Solid_3.22 [46] using a fibre-flexure model (on the left), and the implemented fibre-shear model (on the right)

4.2 Verification against experimental results on short piers with hollow cross-section

A second set of analyses focused on modelling the response of squat RC columns with hollow cross-section (labelled as "Col_Hollow_"). In what follows, two case-studies are presented. The first example is the pier tested by Pinto *et al*. [47] at the European Laboratory for Structural Assessment (ELSA) – Col_Hollow_1.75. The same example has been analysed in detail by Pinto *et al.* [6], Ranzo and Petrangeli [7], Petrangeli [8] and Martinelli [9], using different types of fibre beam elements for shear modelling. The second simulation makes use of the results on piers tested at the University of Pavia [48] – Col_Hollow_2.0. Geometry and material properties of these two hollow columns are summarised in Table II.

Table II. Geometry and material parameters for hollow cross-section squat columns

	Col_Hollow_1.75 L = 2800 mm	Col_Hollow_2.0 L = 900 mm
Reference	Pinto *et al*.[47]	Calvi *et al*.[48]
Scale factor	1:1	1:4
Outer perimeter $b_o \times h_o$ (mm)	800 × 1600	450 × 450
Inner perimeter $b_i \times h_i$ (mm)	480 × 1280	300 × 300
Aspect ratio L/h_o	1.75	2.0
Axial load (kN)	-1700	-250
Concrete strength (MPa)	-35.4	-35.0
Strain at peak stress	-0.0025	-0.0025
Concrete elastic modulus (MPa)	27964	27806
Cracking stress (MPa)	1.96	1.95
N° Long. bars and ϕ (mm)	40 ϕ 8 + 28ϕ 12 + 12 ϕ 10	24 ϕ 8
Long. yielding stress (MPa)	503 & 558 & 489	520
Stirrups ϕ and @ (mm)	ϕ 5@ 60	ϕ 3@ 75
Trans. yielding stress (MPa)	700	710

The force-displacement responses of Col_Hollow_1.75 and Col_Hollow_2.0 are plotted in Figure 12 and Figure 13, respectively, comparing the experimental results with the performed numerical simulations – with flexure modelling (on the left), and with shear modelling (on the right).

The developed modelling strategy seems to be capable of reproducing the measured responses in a satisfactory way, mainly for the Col_Hollow_1.75. Despite the overestimation of the initial stiffness in specimen Col_Hollow_2.0, the flexure-shear model still leads to improved predictions of the overall response if compared with the predictions obtained with the flexural fibre model. However, the model is not able to capture well the degradation of the strength and stiffness for the high ductility levels.

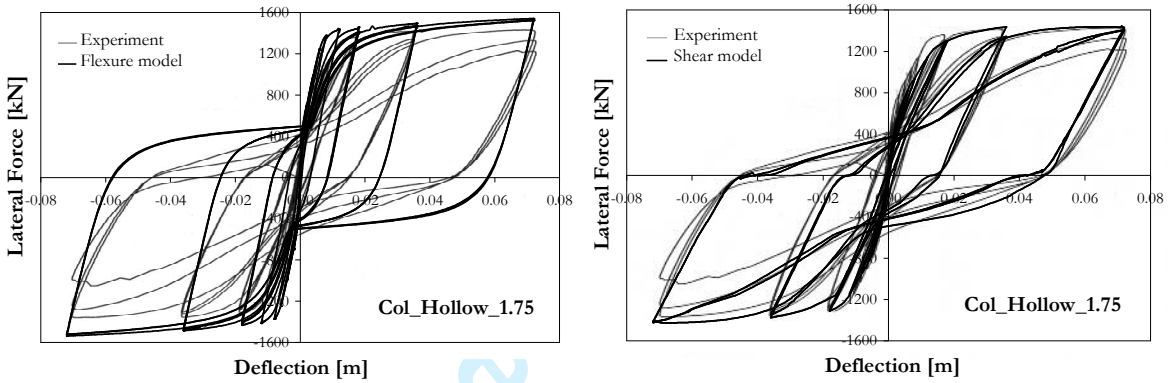

Figure 12. Force-displacement response of specimen Col_Hollow_1.75 [47] using a fibre-flexure model (on the left), and the implemented fibre-shear model (on the right)

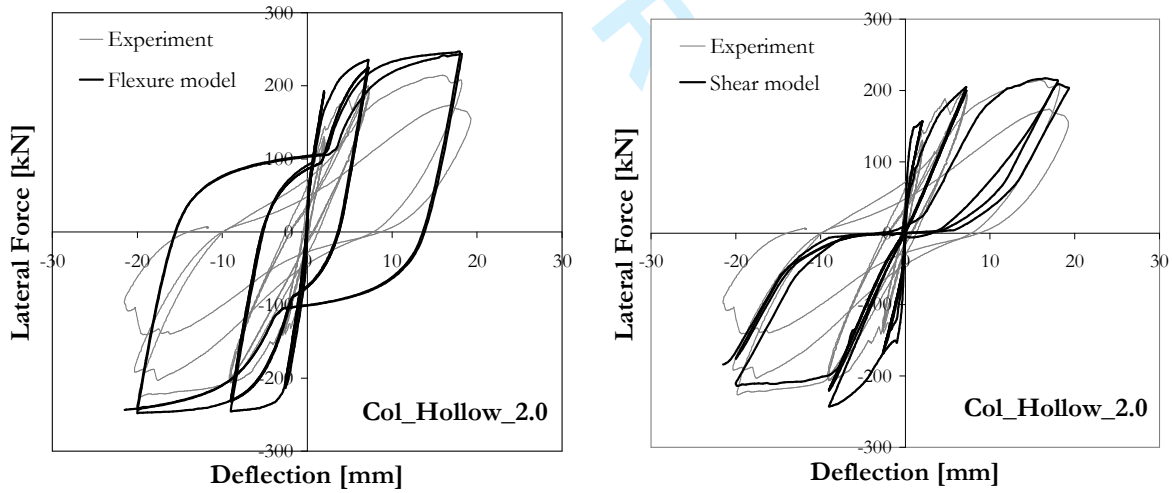

Figure 13. Force-displacement response of specimen Col_Hollow_2.0 [48] using a fibre-flexure model (on the left), and the implemented fibre-shear model (on the right)

4.3 Verification against experimental results on walls

The performance of the developed modelling strategy has also been assessed against the results of two RC structural walls (labelled as "Wall_"). The first results herein discussed refer to a RC specimen (SW35) from the experimental programme of Elnashai and Salama [49] carried out at the Imperial College London. The second validation refers to one of the RC walls (WSH3) tested by Dazio *et al*. [50] at the Swiss Federal Institute of

Technology (ETH) of Zurich. The same example was analysed by Martinelli [10], using a different type of fibre beam element for shear modelling. In the following, the specimens will be named after their aspect ratio as: Wall_2.0, Wall_2.28, respectively.
The geometry and the mechanical properties of the two walls are given in Table III. The numerical simulations of the hysteretic responses of the Wall_2.0 and Wall_2.28 with the flexure and the shear models are shown in Figure 14 and Figure 15, respectively.

Table III. Geometry and material parameters for RC shear walls

	Wall_2.0 L = 1200 mm	Wall_2.28 L = 4560 mm
Reference	Elnashai and Salama[49]	Dazio *et al.*[50]
Scale factor	1:2.5	1:2
Outer perimeter $b_w \times l_w$ (mm)	60 × 600	150 × 2000
Aspect ratio	2.0	2.28
Axial load (kN)	-0.2	-626
Concrete strength (MPa)	-48.4	-39.4
Strain at peak stress	-0.0022	-0.0022
Concrete elastic modulus (MPa)	32698	35700
Cracking stress (MPa)	2.29	2.07
Web - N° Long. bars and ϕ (mm)	6 ϕ 12 + 4 ϕ 6	22 ϕ 8
Long. yielding stress (MPa) of ϕ 8	450	700.2
Egde - N° Long. bars and ϕ (mm)	4 ϕ 8 + 2 ϕ 12	6ϕ 12
Long. yielding stress (MPa) of ϕ 12	450	725.5
Web - Stirrups ϕ and @ (mm)	ϕ 5@ 60	ϕ 6 @150
Edge - Stirrups ϕ and @ (mm)	ϕ 5@ 60 + ϕ 5@ 20	ϕ 6 @150 + ϕ 6 & ϕ 4.2 @75
Trans. yielding stress (MPa) of ϕ 6	450	615
Trans. yielding stress (MPa) of ϕ 4.2	450	552.5

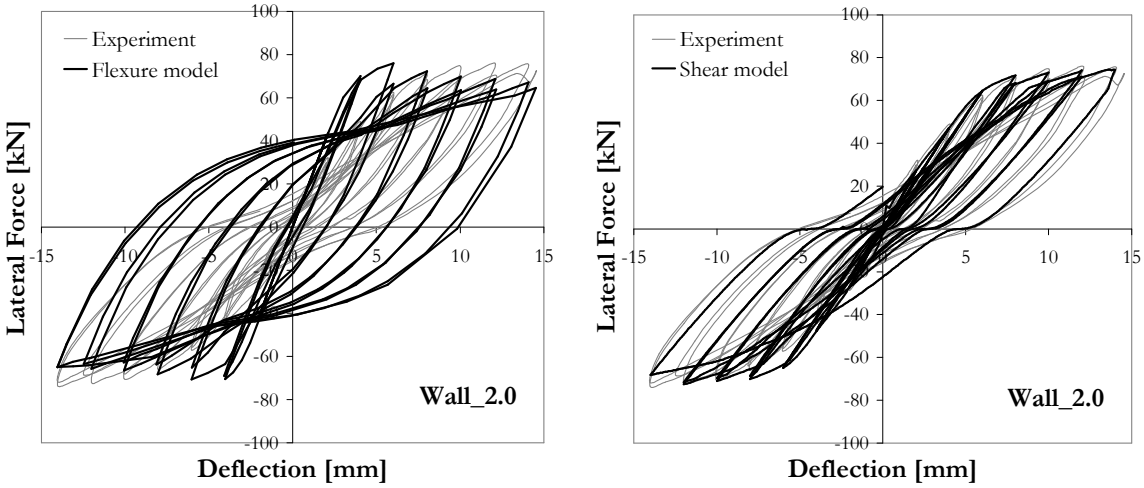

Figure 14. Force-displacement response of specimen Wall_2.0 [49] using a fibre-flexure model (on the left), and the implemented fibre-shear model (on the right)

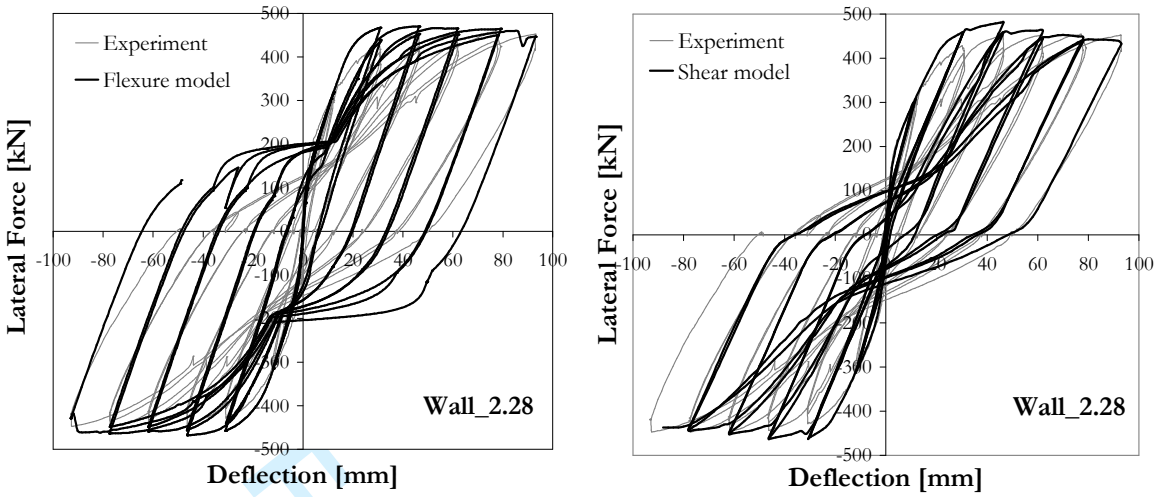

Figure 15. Force-displacement response of specimen Wall_2.28 [50] using a fibre-flexure model (on the left), and the implemented fibre-shear model (on the right)

Once again, it can be observed that the fibre-shear model allows the experimental results to be reproduced with relatively good accuracy, this time without a conspicuous initial stiffness overestimation, as had been observed for the case of columns.

5. CONCLUSIONS

The present research featured the objective of developing a fibre flexure-shear model for seismic analysis of reinforced concrete framed structures. The work started with the assessment of the existing fibre beam-column elements developed in order to account for shear. Further effort was required for the choice of a formulation for cracked reinforced concrete accounting for shear effects, under monotonic and cyclic loading conditions.

A bi-axial fibre constitutive model was developed according to the Modified Compression Field Theory (MCFT). The shear constitutive model was implemented and then verified with comparisons against experimental results. In particular, several RC panel and membrane elements tested at the University of Toronto were considered. The shear constitutive model was then implemented into a fibre beam-column element, after the development of the formulation for the section state determination. The 2D Timoshenko fibre element was formulated according to a displacement-based approach. To avoid shear locking phenomena, the linear shape functions were enriched by the introduction of a bubble function.

The flexure-shear formulation was verified against experimental tests on RC short piers with solid and hollow cross-sections, and on RC rectangular walls. Comparisons with experimental results on these shear-sensitive elements showed relatively good improvement in response "predictions" when the flexural formulation is replaced by the developed fibre-shear formulation. It is also recalled that the developed model does not require empirical test-matching calibration; only engineering parameters (e.g. material strengths, reinforcement geometrical ratios) are required as input.

Nonetheless, numerical difficulties were encountered, mainly associated to initially unknown limitations of the employed constitutive model. Further, post-peak strength degradation is not yet fully captured. Hence, the nonlinear constitutive model

implemented for concrete requires additional improvements; e.g. better post-peak behaviour and a crack-closing model. Additional experimental testing is also likely to be necessary to corroborate the cyclic relationships for concrete in tension and for developing a plastic tensile offset model in order to improve the simulation of the pinching phenomenon. Finally, extension to 3D loading is also to be carried out. In other words, notwithstanding the relatively satisfactory results, it is recognised that further research work and developments are still very much required.

ACKNOWLEDGEMENTS

The authors are very grateful to Prof. Ferdinando Auricchio and Mr. Antonio Araujo Correia for their assistance in the implementation of the developed flexure-shear model into displacement-based and force-based beam-column element formulations, respectively. The authors would also like to thank Prof. Frank Vecchio and Dr. Dan Palermo for the useful comments and observations made regarding the use of the computer code VecTor2. Finally, the authors thank Jesus Bairan, Constantin Christopoulos, Panagiotis Kotronis, Luca Martinelli, Panagiotis Mergos, Dan Palermo, Pierre Pegon, Artur Pinto and Marco Remino for providing valuable bibliographic material related to the current endeavour.

REFERENCES

1. Chan EC. Nonlinear geometric, material and time-dependent analysis of reinforced concrete shells with edge beams. *PhD Thesis* 1982, University of California, Berkeley.
2. Scordelis AC. Computer models for nonlinear analysis of reinforced and prestressed concrete structures. *PCI Journal* 1984; **29**(6).
3. Izzuddin BA. Nonlinear Dynamic Analysis of Framed Structures. *PhD Thesis* 1991, Imperial College, University of London, London, UK.
4. Spacone E, Limkatanyu S. Response of RC members including bond-slip effects. *ACI Structural Journal* 2000; **6**: 831-839.
5. Pinho R, Elnashai AS. Dynamic collapse testing of a full-scale four storey RC frame. *ISET Journal of Earthquake Engineering* 2000; **37**(4): 143-164.
6. Guedes J, Pinto AV. A Numerical Model for Shear Dominated Bridge Piers. *Proceedings of the 2nd Italy-Japan Workshop on Seismic Design and Retrofit of Bridges* 1997, Rome, Italy.
7. Ranzo G, Petrangeli M. A Fibre Finite Beam Element with Section Shear Modelling for Seismic Analysis of RC Structures. *Journal of Earthquake Engineering* 1998; **2**: 443-473.
8. Petrangeli M. Fiber Element for Cyclic Bending and Shear of RC Structures. II: Verification. *Journal of Engineering Mechanics* 1999; **125**(9): 1002-1009.
9. Martinelli L. The Behavior of Reinforced Concrete Piers under Strong Seismic Actions. *Proceedings of the 12th Word Conference on Earthquake Engineering* 2000, Auckland, New Zealand.
10. Martinelli L. Numerical simulation of cyclic tests of R/C shear walls. *Proceedings of the 12th European Conference on Earthquake Engineering* 2002, London, United Kingdom.
11. Marini A, Spacone E. Analysis of Reinforced Concrete Elements Including Shear Effects. *ACI Structural Journal* 2006; **103**(5): 645-655.
12. Bentz EC. Sectional Analysis of Reinforced Concrete Members. *PhD thesis* 2000, University of Toronto, Toronto, Canada.
13. Bairan JM, Mari AR. Coupled model for the nonlinear analysis of anisotropic sections subjected to general 3D loading. Part 1: Theoretical formulation. *Computers and Structures* 2006; **21**: 2254-2263.
14. Kotronis P, Mazars J. Simplified modelling strategies to simulate the dynamic behaviour of R/C walls. *Journal of Earthquake Engineering* 2005; **9**(2): 285-306.

15. Saritas A. Mixed formulation frame element for shear critical steel and reinforced concrete members. *PhD Thesis* 2006, University of California, Berkeley.
16. Gregori JN, Sosa PM, Prada MAF, Filippou FC. A 3D numerical model for reinforced and prestressed concrete elements subjected to combined axial, bending, shear and torsion loading. *Engineering Structures* 2007; **29**: 3404-3419.
17. Ceresa P, Petrini L, Pinho R. Flexure-shear fibre beam-column elements for modelling frame structures under seismic loading- State of the art. *Journal of Earthquake Engineering* 2007; **11**(1): 46-88.
18. Ceresa P. Development of a fibre flexure-shear model for seismic analysis of RC framed structures. *PhD Thesis* 2007, University of Pavia, Pavia, Italy.
19. Collins MP. Towards a rational theory for RC members in shear. *ASCE Journal of Structural Division* 1978; **104**(4): 649-666.
20. Vecchio FJ, Collins MP. The Modified Compression Field Theory for Reinforced Concrete Elements Subjected to Shear. *ACI Journal* 1986; **83**(2): 219-231.
21. Belarbi A, Hsu TTC. Constitutive laws of softened concrete in biaxial tension-compression. *ACI Structural Journal* 1995; **92**(5): 562-573.
22. Pang XB, Hsu TTC. Fixed-angle softened-truss model for reinforced concrete. *ACI Structural Journal* 1996; **93**(2): 197-207.
23. Kaufmann W, Marti P. Structural Concrete: Cracked Membrane Model. *Journal of Structural* Engineering 1998; **124**(12): 1467-1475.
24. Zhu RH. Softened membrane model of cracked reinforced concrete considering the Poisson effect. *PhD Thesis* 2000, Department of Civil and Environmental Engineering, University of Houston, Houston, Texas.
25. Vecchio FJ. Disturbed Stress Field Model for Reinforced Concrete: Formulation. *Journal of Structural Engineering* 2000; **126**(9): 1070-1077.
26. Vecchio FJ. Mechanics of reinforced concrete. *Lecture Notes* 2005, University of Brescia, Brescia, Italy.
27. Vecchio FJ. Towards Cyclic Load Modelling of Reinforced Concrete. *ACI Structural Journal* 1999; **96**(2): 193-202.
28. Palermo D, Vecchio FJ. Compression Field Modelling of Reinforced Concrete subjected to Reversed Loading: Formulation. *ACI Structural Journal* 2003; **100**(5): 616-625.
29. Palermo D, Vecchio FJ. Behavior and Analysis of Reinforced Concrete Walls Subjected to Reversed Cyclic Loading. *Publications No. 2002-01*, Department of Civil Engineering, University of Toronto, Canada, 2002.
30. Vecchio FJ. *Personal communication*, 2007.
31. Wong PS, Vecchio FJ. VecTor2 and Formworks user's manual. *Report* 2002. Civil Engineering, University of Toronto, Toronto, Canada. (Release version: VT2.8F)
32. Seckin M. Hysteretic Behaviour of Cast-in-Place Exterior Beam-Column-Slab Subassemblies. *PhD Thesis* 1981, Department of Civil Engineering, University of Toronto, Canada.
33. Collins MP, Porasz A. Shear design for HSC. *CEB Bulletin* 1989; **193**: 77-83.
34. Stevens NJ, Uzumeri SM, Collins MP. Analytical Modelling of Reinforced Concrete Subjected to Monotonic and Reversed Loadings. *Publications No. 87-01*, Department of Civil Engineering, University of Toronto, Toronto, Canada, 1987.
35. Vecchio FJ, Lai D, Shim W, Ng J. Disturbed Stress Field Model for Reinforced Concrete: Validation. *Journal of Structural Engineering* 2001; **127**(4): 350-358.
36. Vecchio FJ, Lai D. Crack shear-slip in reinforced concrete elements. *Journal of Advanced Concrete Technology* 2004; **2**(3): 289-300.
37. Villani DR. Reinforced concrete subjected to cyclic loads: A pilot study. *BSc Thesis* 1995, Department of Civil Engineering, University of Toronto, Canada.
38. Taylor RL. FEAPpv – A Finite Element Analysis Program: Personal Version. Available freely from the URL http://www.ce.berkeley.edu/~rlt/feappv/ [2005].

39. Prathap G, Bhashyam GR. Reduced integration and the shear flexible beam element. *International Journal of Numerical Methods Engineering* 1982; **18**: 195-210.
40. Auricchio F. Nonlinear finite element analysis. *Class Notes* 2003, ROSE School, Pavia Italy.
41. SeismoSoft. SeismoStruct – A computer program for static and dynamic nonlinear analysis of framed structures (online). Available from URL: www.seismosoft.com [2005]
42. Ceresa P, Petrini L, Pinho R, Auricchio F, Romain S. A fibre flexure-shear model for seismic analysis of RC frame structures. *Research Report ROSE-2008/06*, IUSS Press, Pavia, Italy, 2008. (in press)
43. Arakawa T, Arai Y, Mizoguchi M, Yoshida M. Shear resisting behavior of short reinforced concrete columns under biaxial bending-shear. Transactions of the Japan Concrete Institute 1989; **11**: 317-324.
44. Imai H, Yamamoto Y. A Study on Causes of Earthquake Damage of Izumi High School Due to Miyagi-Ken-Oki Earthquake in 1978. *Transactions of the Japan Concrete Institute* 1986; **8**: 405-418.
45. Aboutaha RS, Engelhardt MD, Jirsa JO, Kreger ME. Rehabilitation of shear critical concrete columns by use of rectangular steel jackets. *ACI Structural Journal* 1999; **96**(1): 68-78.
46. Lynn A. Seismic Evaluation of Existing Reinforced Concrete Building Columns. *PhD Thesis* 1999, University of California at Berkeley, Berkeley, California.
47. Pinto AV, Verzeletti G, Negro P, Guedes J. Cycling Testing of a Squat Bridge Pier. *Report EUR 16247 EN*, EC, JRC, Ispra, Italy, 1995.
48. Calvi GM, Pavese A, Rasulo A, Bolognini D. Experimental and numerical studies on the seismic response of R.C. hollow bridge piers. *Bulletin of Earthquake Engineering* 2005; **3**: 267-297.
49. Elnashai AS, Salama AI. Selective repair and retrofitting techniques for RC structures in seismic regions. *Research Report ESEE/92-2*, Engineering Seismology and Earthquake Engineering Section, Imperial College, London, 1992.
50. Dazio A, Wenk T, Bachmann H. Versuche an Stahlbetontragwanded unter zyklischstatischer Einwirkung. *IBK Bericht N° 239*, ETH Zurich. Basel: Birkhauser Verlag, 1999. (in German)